https://doi.org/10.5194/wes-2024-123
Preprint. Discussion started: 28 October 2024

WIND ENERGY SCIENCE DISCUSSIONS

Gulf of Mexico Hurricane Risk Assessment for Offshore Wind Energy Sites

Lauren A. Mudd[1], Peter J. Vickery[2]

[1]Applied Research Associates, Inc., 8537 Six Forks Rd, Suite 600, Raleigh, NC 27615 ORCID: 0009-0009-1936-7551
[2]Peter J Vickery Consulting, 10101 Grafton Rd, Raleigh, NC 27615, ORCID: 0000-0003-0625-1102

Correspondence to: Lauren A. Mudd (lmudd@ara.com)

Abstract. A feasibility assessment of offshore wind in the Gulf of Mexico conducted by the National Renewable Energy Laboratory concluded that hurricane risk was one of the major challenges that would need to be overcome for a mature offshore wind industry to develop in the Gulf of Mexico as the hurricanes that frequent this area can potentially exceed design limits prescribed by the International Electrotechnical Commission (IEC) wind design standards. To better understand and account for these unique conditions, we target two objectives. The first was to develop a translation between the well-established Saffir-Simpson hurricane scale and the IEC design classes, which are based upon different averaging periods and reference heights and often lead to misinterpretation, speculation, and uncertainty. The conversion of wind speed averaging times between Saffir-Simpson and IEC design standards reflects the behavior of the sea surface drag coefficient as a function of the mean wind speed, which controls the turbulence characteristics of the hurricane boundary layer near the surface. The second objective was to quantify the hurricane exposure risk for wind turbines at sites potentially impacted by hurricanes in the Gulf of Mexico using probabilistic hurricane track and wind field models. The IEC prescribes the reference wind speeds associated with Class 1A and Typhoon Class limit states to be 50 years, though model results indicate the return periods associated with the IEC Class 1A limit state range from approximately 20 to 45 years, while the return periods associated with the Typhoon Class limit-state range from approximately 40 to 110 years. Ultimately, this indicates the Class 1A limit state may be non-conservative for the entire Gulf of Mexico Offshore Wind Energy area, while the Typhoon Class limit-state may be adequate for the design of turbines in some regions of the Gulf of Mexico Offshore Wind Energy area.

1 Introduction

To ensure the robust design of wind turbines in the Gulf of Mexico, it is critical to understand the added risk posed by the threat of major hurricanes, as those affecting the Gulf of Mexico region have a significant potential to exceed design limits prescribed by the International Electrotechnical Commission (IEC) wind design standards.

To satisfy this charge, this project defines the wind hazard for the Gulf of Mexico Offshore Wind Energy area using the hurricane hazard model develop by Applied Research Associates and published extensively in the open literature. In doing so, the return periods associated with the IEC Class 1A and Typhoon Class limit-state hurricanes are estimated on a grid with

https://doi.org/10.5194/wes-2024-123
Preprint. Discussion started: 28 October 2024

nominal resolution of 10 km to determine where hurricane risk results in the exceedance of the IEC design criteria. On the same grid, wind speeds hazard contours associated with a return period of 50 years is also estimated.

An additional challenge in assessing hurricane wind speed risk in the Gulf of Mexico arises from inconsistent terminology across the Saffir-Simpson hurricane scale and the IEC design criteria. Saffir-Simpson definitions are based on 1-minute sustained wind speeds estimated at 10-m height over marine terrain, while the IEC uses a different averaging period (3-second versus 1-minute) and reference height (assumed herein a hub height of 150 m versus 10 m). Employing the latest research on turbulence characteristics of the hurricane boundary layer, conversions between various durations (e.g., 3-seconds, 1-minute, 10-minute, 1-hour) and between elevations near the surface (10 m) to near hub height (assumed herein 150 m) are developed. IEC Class 1A and Typhoon Class limit states are also provided in terms of an equivalent Saffir-Simpson hurricane wind speed category.

2 Harmonizing Hurricane Terminology for Offshore Wind Design

Wind speeds specified in various design codes and those reported by the U.S. Weather Service are often associated with different averaging times. For example, the International Electrotechnical Commission (IEC) specifies a 10 minute average wind speed over an open water surface, whereas the U.S. wind loading standard, American Society of Civil Engineers (ASCE) 7, specifies a 3-second gust wind speed over open land and the U.S. Weather Service specifies a 1-minute average wind speed, where in the case of a hurricane, the wind speed is usually associated with an open water terrain. In all cases the specified wind speeds are at a height of 10 m. In the case of hurricanes, the conversion is wind speed dependent, and in all cases the conversion factors vary with height. Here, we present an approach for converting a wind speed specified with one averaging time to another averaging time to allow better comparisons between IEC wind turbine standards and the Saffir-Simpson hurricane categories.

The conversion of wind speed averaging times from one averaging time to another (e.g., from a 1-minute average to a 3-second gust) requires information on the turbulence characteristics of the hurricane boundary layer. The relevant turbulence characteristics are the turbulence intensity and the velocity spectrum, both of which near the surface only depend on height and the surface roughness. The surface roughness is a function of the mean wind speed and the surface drag coefficient. In addition to controlling the turbulence characteristics of the wind, the sea surface drag coefficient also controls the vertical shear, or rate of change of wind speed with height. The behavior of the surface drag coefficient as a function of wind speed and wave parameters has received significant attention since the pioneering study by Powell et al. (2003). Powell et al. (2003) showed that the drag coefficient reaches a maximum for mean wind speeds at a height of 10 m above mean sea level (U_{10}) in the range of 20 to 30 meters per second (m/s), and then decreases with increasing wind speed. Here we review many of the studies examining the sea surface drag coefficient published since 2003 to determine the model that best describes the behavior of the sea surface drag coefficient as a function of the mean wind speed.

https://doi.org/10.5194/wes-2024-123
Preprint. Discussion started: 28 October 2024

2.1 Sea Surface Drag Coefficient

The sea surface drag coefficient in Powell et al. (2003) was developed by computing the variation of the mean wind speed with height over the lower 500 m of the hurricane boundary layer and then fitting the results of the lower 100 m to 200 m with a logarithmic boundary layer model, from which the aerodynamic surface roughness is obtained. The profiles were grouped into 10 m/s "bins," based on the mean wind speed averaged over the lowest 500 m. Wind speeds were obtained from Global Positioning System (GPS) dropsondes falling through the boundary layer. Details on the computation of wind speeds from dropsondes are given in Hock and Franklin (1999). In addition to Powell et al. (2003), the dropsonde and mean velocity profile approach, or flux-profile method, was used by Vickery et al. (2009a), Holthuijsen et al. (2012), Richter et al. (2016), and Ye et al. (2022).

Assuming a logarithmic profile, the variation of the mean wind speed with height, U(z), is given as

$$U(z) = \frac{u_*}{k}\ln\left(\frac{z}{z_0}\right) \quad (1)$$

where u_* is the friction velocity, k is the von Karmen constant (k=0.4), z is height, and z_0 is the aerodynamic surface roughness. From Eq. 1, it is seen at $z = z_0$ the mean wind speed equals zero. The surface shear stress, τ_0, is defined as

$$\tau_0 = \rho u_*^2 = \rho C_{d_{10}} U_{10}^2 \quad (2)$$

where $C_{d_{10}}$ is the sea surface drag coefficient referenced to U_{10}. Combining Eq. 1 and Eq. 2 yields

$$C_{d_{10}} = \left[k/\ln\left(\frac{10}{z_0}\right)\right]^2 \quad (3)$$

Thus, given z_0, it is straightforward to compute $C_{d_{10}}$. Examples of profiles fitted to the logarithmic profile to estimate z_0 are shown in Figure 1.

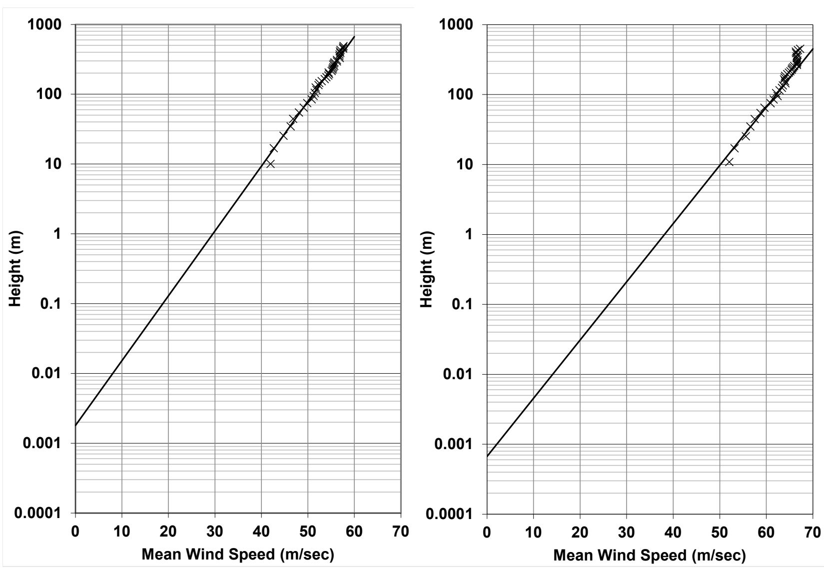

Figure 1: Example measured and fitted velocity profiles. Profiles fitted using method of least squares over a height range of 20 m to 150 m. Computed surface roughnesses in these examples are 0.0018 m and 0.00067 m for the left and right plots, respectively.

https://doi.org/10.5194/wes-2024-123
Preprint. Discussion started: 28 October 2024

Figure 2 presents a plot of $C_{d_{10}}$ vs. U_{10} obtained from the data given in Powell et al. (2003), Vickery et al. (2009a), Holthuijsen (2012), Richter et al. (2016), and Ye et al. (2022).

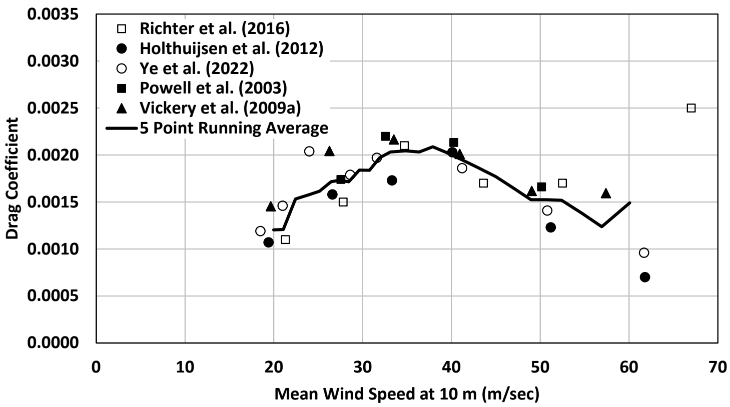

Figure 2: Variation of $C_{d_{10}}$ in tropical cyclones with mean wind speed from various studies obtained using the flux-profile method using GPS dropsondes plotted vs. U_{10}.

Gao et al. (2021), using an eddy-covariance method with data from aircraft flying through tropical cyclones, suggests that $C_{d_{10}}$ reaches a maximum of 1.20×10^{-3} at a saturation wind speed of 33.5 m/s. However, the maximum wind speed in their data is only 28 m/s, and the saturation wind speed of 33.5 m/s was determined using the results of other studies. Vickers et al. (2013) also used aircraft eddy-covariance measurements to determine the relationship between $C_{d_{10}}$ and wind speed and found that $C_{d_{10}}$ reaches a maximum of about 2.3×10^{-3} at a mean wind speed of about 19 m/s. The data show a decrease in $C_{d_{10}}$ as the wind speed increased beyond 19 m/s, but the maximum wind speed is only 23 m/s.

Laboratory studies performed by Takagaki et al. (2012) suggest that the drag coefficient reaches a maximum of about 2.58×10^{-3} for wind speeds greater than about 33 m/s. Donelan et al. (2004), also using laboratory studies, found that $C_{d_{10}}$ reaches a maximum of about 2.5×10^{-3} at U_{10} equals 33 m/s. Note that Curcic and Haus (2020) found an error in the computer code used in the Donelan et al. (2004) paper, changing the saturation speed from 33 m/s to 29 m/s and increasing the limiting value of $C_{d_{10}}$ from 2.5×10^{-3} to 3.0×10^{-3}. Troitskaya et al. (2012) also performed laboratory studies finding that the drag coefficient reaches a maximum of about 2.5×10^{-3} but for U_{10} of about 50 m/s. Lee et al. (2022) suggest that laboratory experiments cannot be used to determine $C_{d_{10}}$ because the effects of wave age, fetch, wavelength, and sea spray are not modeled.

Using data from both laboratory and full-scale, Donelan (2018) suggests that in addition to a wind speed dependence, $C_{d_{10}}$ is a function of the wind-sea Reynolds number, R_B, and wave age and that the reduction in drag coefficient above 30 m/s is largely associated with a wave sheltering effect, where a downstream trough is sheltered by flow separation at the crest of a wave thereby reducing the skin stress in the wave trough. The wind-sea Reynolds number, R_B, is defined as

https://doi.org/10.5194/wes-2024-123
Preprint. Discussion started: 28 October 2024

$$R_B = \frac{u_*^2}{\omega_p \upsilon} = \frac{T_s u_*^2}{2\pi\upsilon} \quad (4)$$

where υ is the kinematic viscosity of sea water and T_s is the significant wave period; wave age, β, is defined as

$$\beta = \frac{c_p}{U_{10}} \quad (5)$$

where c_p is the phase speed of the waves. In deep water, c_p is obtained from

$$c_p = \frac{g}{\omega} = \frac{gT_s}{2\pi} \quad (6)$$

Hsu et al. (2019) also suggest that $C_{d_{10}}$ is a function of the waves, specifically suggesting that $C_{d_{10}}$ is a function of the parameter ζ, defined as

$$\zeta = \frac{gT}{|U_{10}|cos\delta} = \frac{g\left(\frac{\chi}{U_h}\right)}{|U_{10}|cos\delta} \quad (7)$$

where g is the acceleration due to gravity, T is the duration the wind blows over a fetch of length χ, δ is the angle between $|U_{10}|$ and the surface waves, and U_h is the translation speed of the hurricane.

Smith and Montgomery (2010, 2014) argue that the log-law does not apply within the eyewall of a hurricane. Consequently, the computation of an effective surface roughness using the approach used in Powell et al. (2003) and others is not valid. However, it could also be postulated that the use of the reduced drag coefficients at high wind speeds coupled with a logarithmic profile produces the correct variation of the mean wind speed with height in or near the eyewall but for the wrong reasons.

Ye et al. (2022) used the profile method to examine the behavior of $C_{d_{10}}$ at high wind speeds, focusing on the region near the RMW. They found the same reduction in $C_{d_{10}}$ with wind speeds found in other studies using the profile method, but they postulated that tropical cyclone dynamics play a role in affecting the validity of the profile method, e.g., as in Smith and Montgomery (2014). Richter et al. (2021), like Smith and Montgomery (2014), conclude that the flux-profile method may not be valid near the eyewall, suggesting that the flux-profile approach leads to an underestimate of the true value of $C_{d_{10}}$.

Some studies have been performed to determine the behavior of $C_{d_{10}}$ as a function of wind speed using measurements of the wind-induced currents in the ocean (e.g., Jaroz et al. 2007; Zou et al. 2018), or storm surge (e.g., Peng and Lee, 2015). In these studies, the modeled wind speed forcing the ocean response had little or no validation, and consequently drag coefficients derived from these studies are not used in the subsequent discussion presented herein.

The reduction in $C_{d_{10}}$ has also been postulated to be a result of sea spray as first suggested in Powell et al. (2003). Others have since addressed the issue using models for momentum transfer related to the formation of spray and its injection into the wind and subsequent falling back into the water. Andreas (2004) argues that $C_{d_{10}}$, including the effects of sea spray, can be modeled using

$$C_{d_{10}} = \left[1 - 6.5 \times 10^{-5}\left(\frac{\rho_w}{\rho_a}\right)u_*^2\right]\left[k/\ln\left(\frac{10}{z_0}\right)\right]^2 \quad (8)$$

https://doi.org/10.5194/wes-2024-123
Preprint. Discussion started: 28 October 2024

where ρ_w and ρ_a are the densities of sea water and air, respectively. Andreas (2004) points out that the use of Eq. 8 is suggestive rather than conclusive, but it demonstrates that the spray term serves to reduce the sea surface drag coefficient. Makin (2005) develops a model for $C_{d_{10}}$ incorporating sea spray and the critical wind speed (33 m/s) implied in Powell et al. (2003). In incorporating sea spray, Makin (2005) also includes some wave parameters in a model for $C_{d_{10}}$, but by ignoring fetch wave parameters can be related to U_{10}. A two-layer model is proposed, with a thin inner sea surface suspension layer and a logarithmic boundary layer above the suspension layer. Makin postulates that the height of the suspension layer is greater than the height of the short breaking waves, which are much less than the significant wave height.

Liu et al. (2012) also developed a model for the sea surface drag coefficient as a function of wind speed and wave age by extending the work of Makin (2005). For large β, the shape of the Liu et al. (2012) model produces a reasonable match to the $C_{d_{10}}$ versus U_{10} characteristics given Powell et al. (2003). However, both Makin (2005) and Liu et al. (2012) use the fact that $C_{d_{10}}$ in Powell et al. (2003) reaches a maximum for U_{10} = 33 m/s and then postulate that the effect of sea spray on $C_{d_{10}}$ can be ignored for U_{10} less than 33 m/s.

Shi et al. (2016), using the two-layer approach, developed a model for the total drag coefficient including the effects of sea spray. The model relates sea spray to R_B and because wave age is needed to compute T_s for the computation of R_B, the shape of the resulting $C_{d_{10}}$ versus U_{10} is different for each wave age examined. The higher the wave age, the lower the magnitude of U_{10} at which $C_{d_{10}}$ reaches a maximum. In the case of a fully developed sea, β=1.2, Shi et al. (2016) indicate that $C_{d_{10}}$ reaches a maximum of about 2.5×10^{-3} at U_{10}~25 m/s. Waves in hurricanes are not fully developed.

Only Vickery et al. (2009a) present $C_{d_{10}}$ data outside the radius to maximum winds (RMW). They used the flux method. These data do not reach a maximum but rather show a slow increase in $C_{d_{10}}$ with wind speed beyond the nominal ~33 m/s threshold. The highest U_{10} for the outside RMW case was about 45 m/s. Considering that outside RMW no decrease in $C_{d_{10}}$ is seen suggests that Smith and Montgomery's (2014) assertion that the log law does not apply near RMW, and the flux method underestimates $C_{d_{10}}$, may be correct. If this is the case, the use of a drag coefficient wind speed relationship such as given in Figure 3 will produce good estimates of the variation of the mean wind speed with height but may underestimate the turbulence.

https://doi.org/10.5194/wes-2024-123
Preprint. Discussion started: 28 October 2024

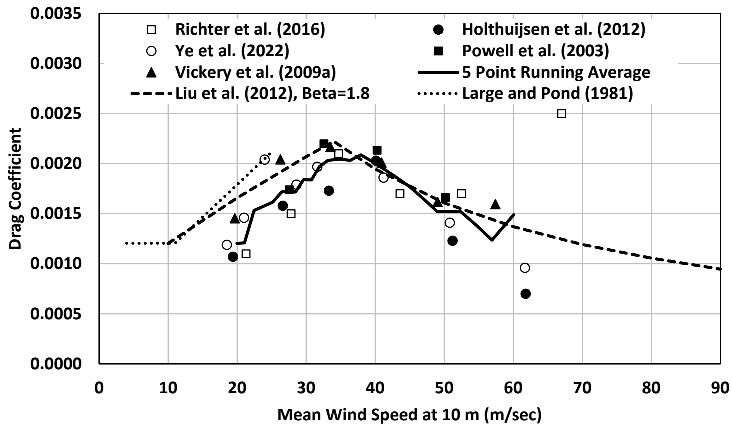

Figure 3: Variation of $C_{d_{10}}$ in tropical cyclones with mean wind speed from various studies obtained using the flux-profile method using GPS dropsondes plus the model given in Liu et al. (2012) and the Large and Pond (1981) model for wind speeds less than 25 m/s

2.2 Gust Factors

The characteristics of the near-surface turbulence within the marine boundary layer are needed to estimate peak wind speeds, turbulence intensities, velocity spectra, and so on. Unfortunately, there are very few detailed public domain measurements of turbulence in hurricanes over the ocean. High-resolution wind speed traces are not stored by the National Oceanic and Atmospheric Administration (NOAA)/National Climatic Data Center, whose data are limited to mean wind speeds (of various durations) and peak gust wind speeds (of various averaging times). Direct passages of the eyewall over a NOAA data buoy or C-MAN station without failures of the anemometry are rare. To date, the highest 10-minute mean wind speed at a NOAA station is 56.4 m/s, which was recorded at C-MAN station FYWF1 during Hurricane Andrew in 1992 at a height of 43.9 m.

2.2.1 Gust Factor Data from He et al. (2020)

He et al. (2020) report marine gust factors for mean wind speeds greater than 70 m/s. These data were recorded during Super Typhoon Hato using wind speed data recorded with an anemometer mounted on a 6.5-m mast, at an elevation of 60 m above sea level on a small island in the South China Sea. The typhoon passed almost directly over the anemometer which experienced high winds approaching first from the northwest and second from the southeast. The location of the anemometer on the island and the approximate range of wind directions associated with each passage of high winds are shown in Figure 4.

https://doi.org/10.5194/wes-2024-123
Preprint. Discussion started: 28 October 2024

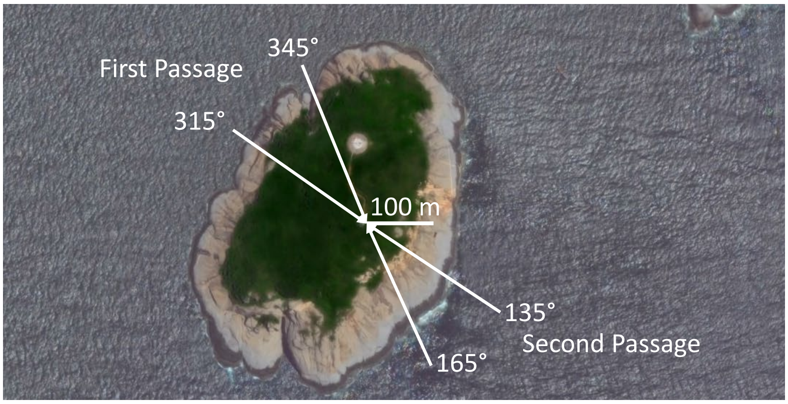

Figure 4: Image of the small island in the South China Sea showing the location of the anemometer and the wind directions associated with the first and second passages of high winds. In the first passage, the anemometer is located about 200 m from the shoreline; for the second passage, the anemometer is about 150 m from the shoreline.

The anemometer recorded the maximum 3-s gust speed and the average 1-minute wind speed every minute. He et al. (2020) used these data to compute the 3-s gust factor defined as the maximum 3-s gust wind speed each minute divided by the 1-minute mean wind speed in each interval. These data were averaged and binned into 10 m/s bins, a summary of which is presented in Table 1.

Table 1: Gust Factor Data from He et al. (2020)

Wind Speed at 66.5 m (m/s)	First Passage			Second Passage		
	N(1)	G(3,60)(2)	Std. Dev.	N(1)	G(3,60)(2)	Std. Dev.
10–15	93	1.16	0.04	62	1.14	0.04
15–20	167	1.17	0.05	82	1.15	0.04
20–30	140	1.20	0.05	73	1.19	0.05
30–40	19	1.28	0.08	32	1.18	0.05
40–50	7	1.33	0.07	32	1.20	0.06
50–60	13	1.26	0.06	6	1.18	0.05
60–70	1	1.17		17	1.15	0.03
70–75				6	1.13	0.03

(1) N = Number of samples

(2) G(3,60) = 3-s peak gust wind speed recorded over a 60-s period divided by the mean wind speed averaged over 60 seconds

The mean gust factors in each bin are plotted versus wind speed in Figure 5. Because the wind speeds were averaged within each bin, the wind speeds represent a long-term (e.g., 10 minutes to an hour); thus, the horizontal axis represents a mean wind speed rather than a 1-minute wind speed—but a precise estimate of the effective averaging time is difficult to ascertain because the 1-minute wind speeds and associated gust factors were sorted before being averaged. Also shown in Figure 5 are the 1-minute gust factors computed using the ESDU (1982, 1983) formulations for the gust factor coupled with the sea

https://doi.org/10.5194/wes-2024-123
Preprint. Discussion started: 28 October 2024

surface drag coefficient computed using three different assumptions. The sea surface drag coefficient models include that proposed by Large and Pond (1981) with maximum values of 0.0019 and 0.0023, and the model of Liu et al. (2012) using β =1.8 (fully developed). The maximum values of 0.0019 and 0.0023 are approximately the lower and upper bounds of the radius-dependent model used for $C_{d_{10}}$ discussed in Vickery at al. (2009a).

The modeled gust factors were computed assuming that the average wind speeds given in Table 1 are representative of a 10-minute mean winds speed (i.e., maximum 10-minute mean within an hour). The gust factors associated with the first and second passages yield similar trends, first increasing with wind speed, reaching a maximum and then decreasing; however, the maximum value of the gust factors from the first and second passages are notably different: The gust factors from the first passage are much higher than those from the second passage for wind speeds between 30 m/s and 50 m/s. It is not clear how the mean and gust wind speeds may have been influenced by the effects of the local terrain and topographic speed-ups induced by the island's terrain and topography. However, for each passage of strong winds, the influence of terrain, fetch, and wind speed-ups would not be expected to vary significantly because the range of directions associated with the strong winds is relatively narrow. The maximum wind speed of 72 m/s at a height of 66.5 m above sea level (ASL) (shown in Figure 5) corresponds to U_{10} of about 61 m/s.

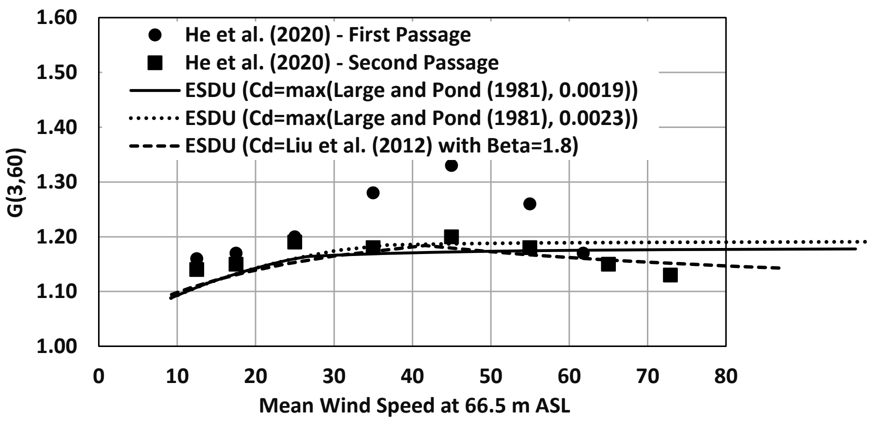

Figure 5: Modeled and measured (He et al. 2020) gust factors in high winds in the South China Sea

Statistics of the differences and the R^2 values associated with the comparison of the three gust factor models to the gust factor data from the second passage shown in Figure 5 are summarized in Table 2. Not surprisingly, the model of Liu et al. (2012), as implemented here, produces the highest R^2, with the R^2 values from both Large and Pond (1981) models being negative. 2.2.2 Gust Factor Data from NOAA Stations

All C-MAN data were collected from hurricanes affecting the Atlantic coast, and all buoy data were from Gulf of Mexico hurricanes. Both C-MANs and buoys report the maximum 5-s gust occurring in a 1-hour period, the time at which the gust occurred, and a 10-minute mean wind speed every 10 minutes. In the case of the buoy data, only data from the 10-m buoys were considered because wind data from buoys with anemometer heights of 3 m and 5 m are thought to have been influenced by the local sea state because they drop into the wave troughs where sheltering is expected.

Table 2: Quantitative Comparisons of Model and Observed Gust Factors, G(3,60) at a Height of 66.5 m. Observed Gust Factors from Passage Two as Given in He et al. (2020).

Drag Coefficient Model	Mean Error	Error Std. Dev	R^2
Large and Pond (1981) with cap of 0.0019	-0.007	0.029	-0.264
Large and Pond (1981) with cap of 0.0023	0.002	0.034	-0.708
Liu et al. (2012) with β = 1.8	-0.012	0.020	0.377

A difficulty encountered when comparing the measured gust factors to modeled gust factors is associated with the lack of stationarity associated with hurricanes, and the fact that there is only one measurement of the gust wind speed during an hour, but there are six 10-minute means hence, five other gust factors that may have (but not necessarily) all been lower than the one computed gust factor, which uses the largest gust wind speed within the hour.

Here, the measured gust factors are defined using two methods:

i) The largest gust recorded during a 1-hour period divided by the 10-minute mean wind speed recorded during the time at which the gust was measured.

ii) The largest gust recorded during a 1-hour period divided by the 30-minute mean wind speed computed using the average of the 10-minute wind speed recorded during the time at which the gust was measured and the 10-minute wind speeds occurring immediately before and after.

C-MAN Gust Factors. The anemometer heights for C-MANs DSLN7, FPSN7, and FWYF1 are 46.6 m, 44.2 m, and 43.9 m, respectively. All gust factor data from these three C-MANs were combined, with the analytic estimates of the gust factor computed using the average height of 44.9 m. Summaries of the gust factors from the C-MANs are presented in Table 3, where the number of samples, and the mean and standard deviation of the gust factor are provided in each wind speed bin.

The difference in the estimates of the gust factor computed using the 10-minute or 30-minute mean wind speeds is negligible, with a maximum difference of less than 1% and an average difference of less than 0.1%, suggesting that the use of the 10-minute mean wind speed within which the hourly peak gust wind speed was recorded is representative of G(5,3600).

Figure 6 presents gust factors computed from wind speed data obtained from the C-MAN stations during hurricanes along with the gust factors computed using the capped Large and Pond (1981) representation of the drag coefficient as well as the drag coefficient described in Liu et al. (2012). There are only ten 10-minute mean wind speeds greater than 40 m/s and only eight 30-minute mean wind speeds greater than 40 m/s.

Table 4 presents the error statistics (difference between the modeled and observed gust factors) for the three different modeled representations of the sea-surface drag coefficient given in Figure 6. The error statistics including the mean error, standard deviation of the error and the R^2. The summary statistics Table 4 indicate that the gust factor at a height of 10-m is best modeled when the sea-surface drag coefficient is modeled using the Large and Pond (1981) model with a cap of 0.0019.

https://doi.org/10.5194/wes-2024-123
Preprint. Discussion started: 28 October 2024

Table 3. Five-second Gust Factors From C-MAN Stations DSLN7, FPSN7, and FWYF1. Measured Gust Factors Computed Using a 10-Minute Mean Wind Speed (left 4 columns) and a 30-Minute Mean Wind Speed (right 4 columns)

U(44.9,600)[(1)] (m/s)	G(5,3600)[(2)]	Std. Dev. (m/s)	Number of Samples	U(44.9,1800)[(3)] (m/s)	G(5,3600)[(4)]	Std. Dev. (m/s)	Number of Samples
12.4	1.24	0.125	249	12.4	1.24	0.138	250
17.2	1.25	0.094	157	17.2	1.24	0.094	156
22.4	1.26	0.084	137	22.2	1.26	0.079	130
27.1	1.31	0.093	78	27.0	1.31	0.098	86
32.4	1.28	0.091	50	32.3	1.27	0.094	49
36.8	1.30	0.102	17	36.4	1.31	0.095	19
43.1	1.25	0.077	8	42.3	1.25	0.071	7
48.5	1.36		1	48.6	1.36		1
56.4	1.34		1				

[(1)] U(44.9,600) = Mean wind speed at a height of 44.9 m averaged over a period of 600 seconds

[(2)] G(5,3600) = = Max. 5-s peak gust recorded during a 3,600-s period divided by the 3,600 second mean wind speed

[(3)] U(44.9,1800) = Mean wind speed at a height of 44.9 m averaged over a period of 1,800 seconds

[(4)] G(5,3600) = = Max. 5-s peak gust recorded during a 3,600-s period divided by the 3,600 second mean wind speed

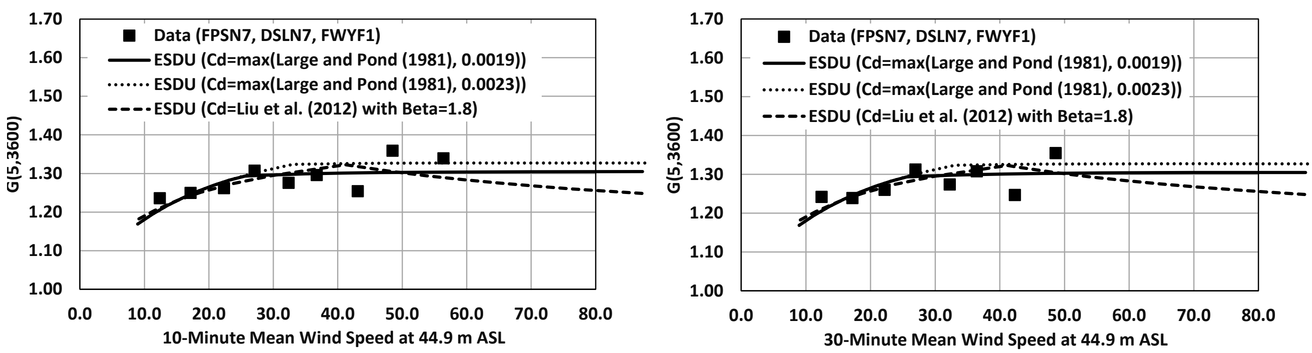

Figure 6. Modeled and measured gust factors at a height of 44.9 m. Measured gust factors from NOAA C-MAN stations based on a 10-minute mean wind speed (left) and a 30-minute mean wind speed (right).

Table 4. Quantitative Comparisons of Model and Observed Gust Factors, G(5,3600), at a Height of 44.9 m. Observed Gust Factors Are From Passage From C-MANs DSLN7, FPSN7, and FWYF1 and Are Computed using both 10-Minute and 30-Minute Mean Wind Speeds.

Drag Coefficient Model	Observation Period (sec)	Mean Error	Std. Dev. of Error	R^2
Large and Pond (1981) with cap of 0.0019	600	-0.002	0.032	0.429
Large and Pond (1981) with cap of 0.0023	600	0.011	0.035	0.320
Liu et al. (2012) with β = 1.8	600	0.00	0.038	0.170
Large and Pond (1981) with cap of 0.0019	1,800	-0.002	0.034	0.321
Large and Pond (1981) with cap of 0.0023	1,800	0.011	0.038	0.157
Liu et al. (2012) with β = 1.8	1,800	0.001	0.038	0.167

Buoy Gust Factors. Summaries of the gust factors from the buoy stations are presented in Table 5, where the number of samples, and the mean and standard deviation of the gust factor are provided in each wind speed bin. As in the case of the gust factors from the C-MAN stations, the difference in the estimates of the gust factor computed using the 10-minute or 30-minute mean wind speeds is small, with a maximum difference of about 2% and an average difference of 0.2%, again suggesting that the use of the 10-minute mean wind speed within which the hourly peak gust wind speed was recorded is representative of G(5,3600). There are only six 10-minute mean wind speeds greater that 40 m/s and eight 30-minute mean wind speeds greater than 40 m/s.

Table 5. Five-S Gust Factors from NOAA 10-m Discus Buoys. Measured Gust Factors Computed Using Both 10-Minute and 30-Minute Mean Wind Speed.

U(10,600)[1] (m/s)	G(5,3600)[2]	Std. Dev. (m/s)	Number of Samples	U(10,1800)[3] (m/s)	G(5,3600)[4]	Std. Dev. (m/s)	Number of Samples
17.0	1.31	0.079	200	17.0	1.33	0.080	212
22.1	1.32	0.069	95	22.2	1.33	0.068	90
27.0	1.32	0.044	57	27.0	1.33	0.038	50
32.5	1.27	0.087	2	32.3	1.28	0.062	2
37.7	1.31	0.091	4	36.3	1.28	0.151	2
41.6	1.38	0.046	3	41.2	1.36	0.063	6
46.6	1.37	0.038	3	47.7	1.38	0.004	2

(1) U(10,600) = Mean wind speed at a height of 10 m averaged over a period of 600 seconds

(2) G(5,3600) = Max. 5-s peak gust recorded during a 3,600-s period divided by the 600 second mean wind speed

(3) U(10,1800) = Mean wind speed at a height of 10 m averaged over a period of 1,800 seconds

(4) G(5,3600) = Max. 5-s peak gust recorded during a 3,600-s period divided by the 1,800 second mean wind speed

https://doi.org/10.5194/wes-2024-123
Preprint. Discussion started: 28 October 2024

Figure 7 presents gust factors computed from wind speed data obtained from the C-MAN stations during hurricanes along with the gust factors computed using the capped Large and Pond (1981) representation of the drag coefficient as well as the drag coefficient described in Liu et al. (2012).

Summary statistics are provided in Table 6, where it is seen that $C_{d_{10}}$ modeled using the Liu et al. (2012) model performs worst and the Large and Pond (1981) formulation with a cap of 0.0019 performs best but still yields a negative R^2. The poor performance of the models is due to the observed apparent outlier gust factors for U_{10} between 30 m/s and 40 m/s.

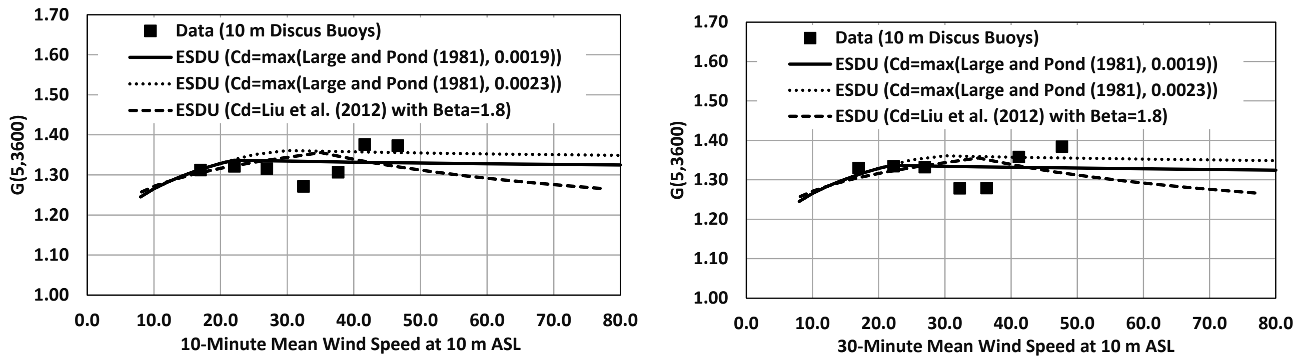

Figure 7: Modeled and measured gust factors at a height of 10.0 m. Measured gust factors from 10-m NOAA discus buoys, based on a 10-minute mean wind speed (left) and a 30-minute mean wind speed (right).

Table 6: Quantitative Comparisons of Model and Observed Gust Factors, G(5,3600), at a Height of 10 m. Observed Gust Factors from 10 m Discuss Buoys Computed Using both 10-Minute and 30-Minute Mean Wind Speeds.

Drag Coefficient Model	Observation Period (sec)	Mean Error	Std. Dev. of Error	R^2
Large and Pond (1981) with cap of 0.0019	600	0.002	0.040	-0.086
Large and Pond (1981) with cap of 0.0023	600	0.021	0.044	-0.303
Liu et al. (2012) with β = 1.8	600	0.002	0.051	-0.629
Large and Pond (1981) with cap of 0.0019	1,800	0.005	0.038	-0.046
Large and Pond (1981) with cap of 0.0023	1,800	0.023	0.040	-0.120
Liu et al. (2012) with β = 1.8	1,800	0.005	0.048	-0.755

2.3 Drag Coefficient Summary

The review of the literature pertaining to the behavior of sea surface drag coefficients as a function of wind speed in hurricanes, coupled with the analysis of gust factors over the ocean in hurricanes, leads to somewhat ambiguous conclusions. There is no direct method to measure the sea surface drag coefficient; therefore, indirect methods are used. Currently, there is no consensus on which of the methods discussed herein yields the most reliable solutions, and there is still significant uncertainty about the behavior of $C_{d_{10}}$ at very high (ultimate design) wind speeds, which largely occur near the eyewall of hurricanes.

https://doi.org/10.5194/wes-2024-123
Preprint. Discussion started: 28 October 2024

The gust factor analysis using NOAA data suggests that the drag coefficient does not reach a maximum for U_{10} around 33 m/s as suggested in Powell et al. (2003) and by extension suggests that $C_{d_{10}}$ is perhaps limited by the action of sea spray but this decrease does not occur, until U_{10} reaches approximately 50 m/s. The analysis of gust factors derived from the NOAA platforms suggests that the model for the sea surface drag coefficient capped at 0.0019 provides the best description of $C_{d_{10}}$. The gust factor data described in He et al. (2022) suggest that $C_{d_{10}}$ decreases for U_{10} greater than about 50 m/s.

Considering the suggestion of Smith and Montgomery (2014) that the flux-profile method may not be valid near the eyewall suggesting that the flux-profile approach leads to an underestimate of the true value of $C_{d_{10}}$, a model for $C_{d_{10}}$ having a maximum value, and not decreasing thereafter, appears to be the most appropriate approach. However, because the mean profiles derived from the dropsondes at high wind speeds appear to be flatter, having a shape consistent with a low $C_{d_{10}}$, it is possible that given U_{10}, the hurricane boundary model used herein overestimates U_{150} but yields reasonable estimates of gust factors.

The relationship between the maximum 1-minute wind speeds at the Saffir-Simpson hurricane category break points and wind speeds associated with other average times at heights of 10 m and 150 m above sea level is given in Table 7. IEC 61400-1 (IEC TC88-MT1 2019) defines the reference wind speed as a 10-minute average wind speed with a return period of 50 years at turbine hub height. The reference wind speed values for Class 1A and Typhoon Class are provided in Table 1 of IEC 61400-1 as 50 and 57 m/s (111.9 and 127. mph), respectively.

According to Table 7 and assuming a hub height of 150 m, the Class 1A reference wind speed is associated with the lower limit of a Category 2 hurricane, and the Typhoon Class reference wind speed is associated with just under the lower limit of a Category 3 hurricane. The IEC 3-s extreme gust criteria, which are 70 m/s for Class 1A turbines and 80 m/s for Typhoon Class turbines, are associated with a strong Category 2 and a moderate Category 3 hurricane, respectively.

Based largely on the gust factor comparisons and the drag coefficient data presented in Figure 3, we suggest that for the lower 100 m to 200 m, that the hurricane boundary layer be modeled using a mean profile described using the log law as given in Equation 1 and a drag coefficient model that uses the Large and Pond (1981) model with an upper limit of 0.0019. This model for $C_{d_{10}}$ results in a relatively low $C_{d_{10}}$ at high wind speeds but does not yield a reduction in $C_{d_{10}}$. The model is possibly conservative; however, until consensus is reached on the behavior of $C_{d_{10}}$ at high wind speeds in hurricanes, we believe that this approach is prudent. The turbulence characteristics of the wind are well modeled using the ESDU (1982, 1983) models for atmospheric turbulence.

https://doi.org/10.5194/wes-2024-123
Preprint. Discussion started: 28 October 2024

Table 7: Wind Speeds in m/s (mph) at the Break Points Between Hurricane Categories. Wind Speeds Are Given at Heights of 10 m and 150 m for Averaging Times of 1 Hour, 10 Minutes, 1 Minute, and 3 Seconds. Wind Speeds Are Computed Using a Sea Surface Drag Coefficient of 0.0019 and the ESDU (1982) Model for the Mean Boundary Layer.

	Category 1	Category 2	Category 3	Category 4	Category 5
Hourly, z=10 m	29.1 (65.2)	37.8 (84.6)	43.7 (97.2)	51.3 (114.7)	62.0 (138.6)
10 Minute, z=10	30.2 (67.6)	39.2 (87.7)	45.4 (101.5)	53.2 (118.9)	64.2 (143.7)
1 Minute, z=10 m	**33.1 (74.0)**	**42.9 (96.0)**	**49.6 (111.0)**	**58.1 (130.0)**	**70.2 (157.0)**
3-Second Gust, z=10 m	39.8 (89.0)	51.5 (115.3)	59.5 (133.2)	69.7 (155.9)	84.1 (188.1)
Hourly, z=150 m	37.7 (84.4)	49.0 (109.5)	56.7 (126.7)	66.4 (148.5)	80.2 (179.5)
10 Minute, z=150	38.9 (86.9)	50.5 (113.0)	58.5 (130.8)	68.6 (153.4)	82.9 (185.5)
1 Minute, z=150 m	42.0 (93.9)	54.8 (122.5)	63.5 (142.1)	74.6 (166.9)	90.4 (202.2)
3-Second Gust, z=150 m	47.2 (105.7)	61.9 (138.4)	71.9 (160.9)	84.7 (189.5)	102.9 (230.1)

3 Hurricane Hazard Modeling

The key components of the hurricane hazard model are i) probabilistic models describing the occurrence rates, storm tracks, and intensities (Vickery et al. 2009b) and ii) the hurricane wind field model (Vickery et al. 2009a). Section 3.1 provides an overview of the track modeling approach and presents validation examples in the Gulf of Mexico region encompassing the Offshore Wind Energy area. For full details on the development and validation of the wind field model, including modelling the variation in wind speed with height, see Vickery et al. (2009a).

3.1 Hurricane Track and Intensity Modeling

The probabilistic portion of the hurricane hazard model is described in detail in Vickery et al. (2000b, 2009b). The key features of the storm track model are the coupling of the modeling of the central pressure with sea surface temperature (SST) and the ability to model curved tracks that can make multiple landfalls. The entire track of a storm is modeled, from the time of storm initiation over the water until the storm dissipates. The starting times (hour, day, and month) and locations of the storms are taken directly from the Atlantic Basin Best Track Data, hereafter HURDAT2 (Landsea and Franklin, 2013). Using the actual starting times and locations ensures that any climatological preference for storms to initiate in different parts of the Atlantic Basin at different times of the year is maintained.

The coupling of the central pressure modeling to sea surface temperature ensures that intense storms (such as Category 5 storms) cannot occur in regions in which they physically could not exist (such as at extreme northern latitudes). As shown in Vickery et al. (2000b, 2009b), the approach reproduces the variation in the central pressure characteristics along the United States coastline. In the hurricane hazard model, the storm's intensity is modeled as a function of the sea surface temperature and wind shear until the storm makes landfall. At the time of landfall, the filling models described in Vickery (2005) are used to exponentially decay the intensity of the storm over land. Over land, following the approach outlined in Vickery et al. (2009b), the storm size is modeled as a function of central pressure and latitude. If the storm exits land into the water, the storm intensity is again modeled as a function of sea surface temperature and wind shear, allowing the storm to possibly reintensify and make landfall again elsewhere.

The validity of the modeling approach for storms near the coastal United States is shown through comparisons of the statistics of historical and modeled key hurricane parameters along the North American coast. Comparisons of occurrence rate, heading, translation speed, distance of closest approach, and so on, are given in Vickery et al. (2009b). These comparisons are made using the statistics derived from historical and modeled storms that pass within 250 kilometers (km) of a coastal milepost location. The comparisons are also given for mileposts spaced 50 nautical miles apart along the entire United States Gulf and Atlantic coastlines. In all comparison figures in Vickery et al. (2009b), the 90% confidence bounds are also plotted and shown to encompass the historical data, indicating with 90% confidence that the historical and modeled data are from equivalent statistical distributions. Results of additional statistical testing using the chi-square, Kolmogorov-Smirnov, and James and Mason tests of equivalent distributions are also provided, indicating that the confidence in equivalent distributions of some track modeling parameters may be as high as 95%. Validation examples are also presented later in this section.

3.1.1 Hurricane Track and Intensity Validation

The HURDAT2 database is used to validate the away from the U.S. coastline. HURDAT2 contains position data (latitudes and longitudes), central pressures, and estimates of the maximum wind speed (maximum 1-minute average wind speed at a height of 10 m) given in increments of 5 knots. Prior to the satellite era (~1970), information on central pressure is limited to near-shore estimates obtained by reconnaissance aircraft. These limited aircraft data are available starting in the mid-1940s. Prior to the aircraft era, estimates of central pressure were derived from ship reports and other ground sources. The HURDAT2 data are archived at 6-hour increments. Furthermore, central pressures other than those at the start and end of each 6-hour segment are not recorded. Therefore, it is unlikely that one these 6-hour positions contain the minimum central pressure experienced over the life of the storm.

In addition to the information obtained from the HURDAT2 data set, the model is validated/calibrated using a separate data set that provides details on landfall pressures (Blake et al. 2011). Both the landfall data set and the HURDAT2 data set are continually being updated through the ongoing HURDAT2 reanalysis project (http://www.aoml.noaa.gov/hrd/data_sub/re_anal.html). The HURDAT2 data set used here includes all revisions to historical storm data through the June 2019 HURDAT2 update.

Figure 8 and Figure 9 present example comparisons of the modeled and historical cumulative distribution functions (CDF) of storm heading (i.e., the direction a storm is traveling) and storm translation speed (i.e., the speed at which a storm is traveling) in the Gulf of Mexico. In addition to the CDFs, Figure 8 and Figure 9 also include a simplified coastline of the western Gulf of Mexico from Mexico to Louisiana as shown by the blue line. Each CDF was developed using information

https://doi.org/10.5194/wes-2024-123
Preprint. Discussion started: 28 October 2024

on all historical tropical cyclones passing within 250 km of a specified latitude-longitude pair. These validation circles are centered on a 2-degree grid, with results presented here encompassing the western Gulf of Mexico from 22°N to 32°N latitude and 90°W to 98°W longitude.

Figure 10 presents example comparisons of modeled and observed central pressures plotted versus return period. For orientation purposes, a simplified coastline of the western Gulf of Mexico from Mexico to Louisiana is also shown by the blue line in Figure 10. The observed central pressures plotted versus return period were computed assuming that the *Np* pressure data points obtained from a total of *N* tropical cyclones that pass through the circle are representative of the full population of *N* storms. With this assumption, the CDF for the conditional distribution for storm central pressure is computed, where each pressure has a probability of 1/(*Np*+1). The return period associated with a given central pressure is obtained from

$$P_t(p_c < P_c) = 1 - \sum_{x=0}^{\infty} P_t(p_c > P_c|x) p_t(x) \tag{9}$$

where $P_t(p_c > P_c|x)$ is the probability that velocity *v* is less than *V* given that *x* storms occur, and $p_t(x)$ is the probability of *x* storms occurring during time period *t*. From Eq. 9, with $p_t(x)$ defined as Poisson and defining *t* as 1 year, the annual probability of exceeding a given wind speed is

$$P_a(p_c < P_c) = 1 - exp[-\lambda P(p_c < P_c)] \tag{10}$$

where λ is the annual occurrence rate defined as N/N_Y where N_Y is the number of years in the historical record, here equal to 120 years (1900 through 2019).

The model estimates of central pressure versus return period for a given location are computed using Eq. 10, where λ is the annual occurrence rate of simulated storms affecting the location of interest (e.g., the number of simulated storms within 250 km of a location divided by the number of simulated years). The probability distribution for central pressure is obtained by rank ordering the simulated central pressures. The comparisons of modeled and observed central pressures given in Figure 10 use the minimum value of the central pressures while a storm (modeled or historical) is within the 250 of the indicated point.

https://doi.org/10.5194/wes-2024-123
Preprint. Discussion started: 28 October 2024

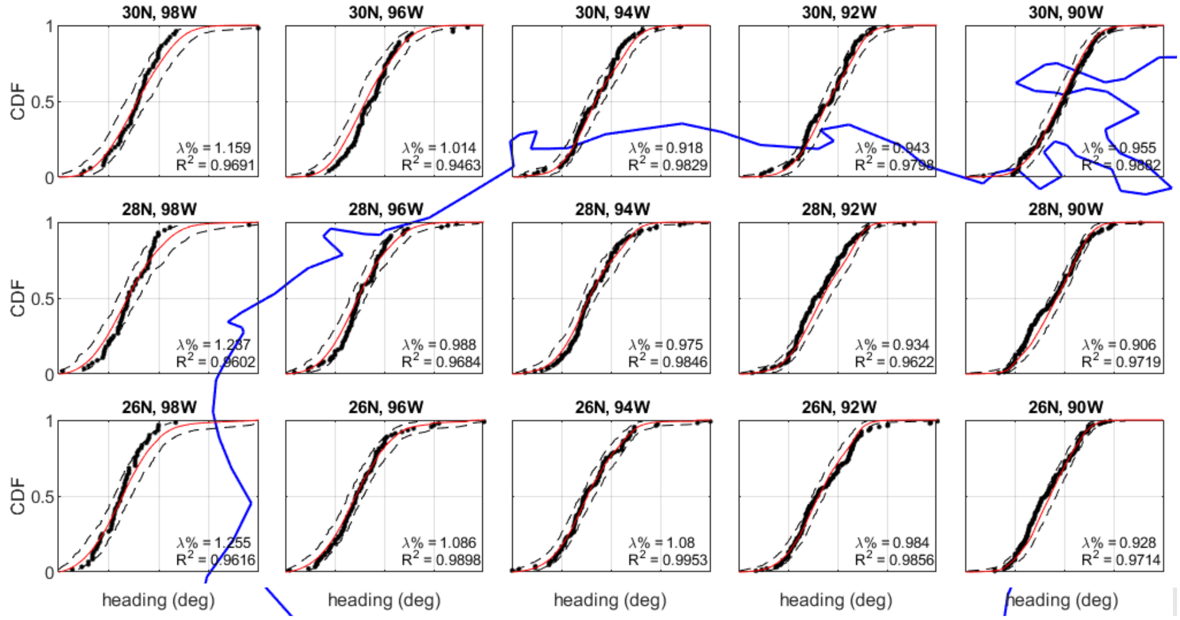

Figure 8. Comparison of the modeled and observed cumulative distribution functions (CDFs) for storm heading. Values are the heading of the storm at the time it was nearest to the center of a 250-km radius circle centered on the point indicated by the title of each graph. Observations are shown by black dots, modeled values are shown by red line, and 95% confidence bounds are shown by dashed black lines. Western Gulf of Mexico coastline is shown by blue line for orientation purposes.

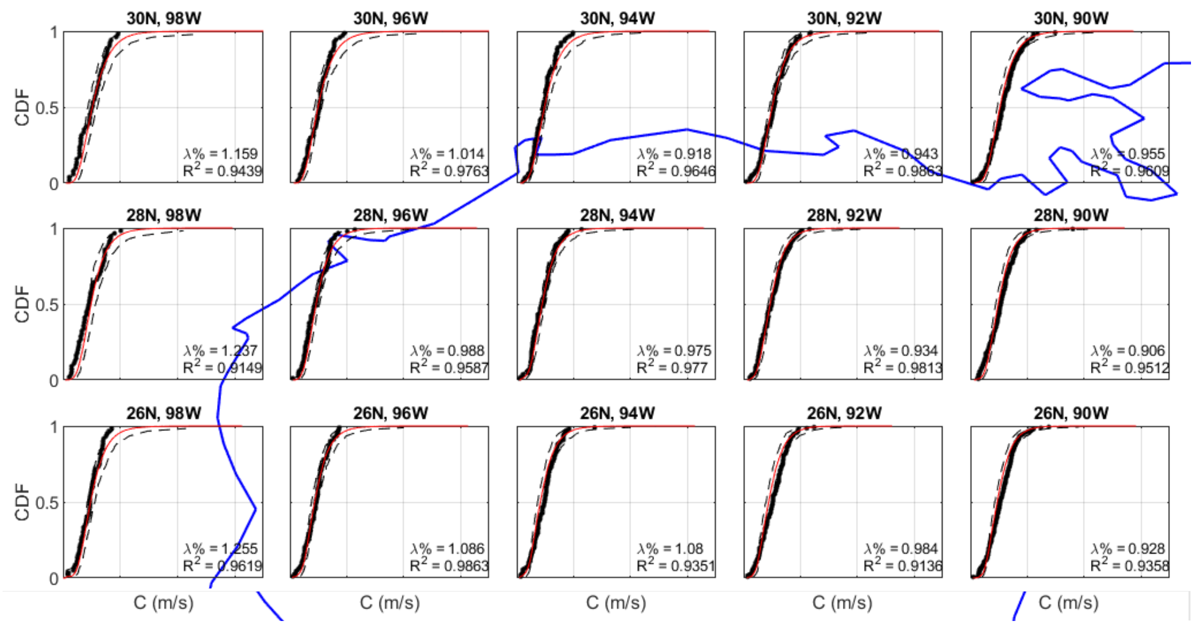

Figure 9. Comparison of the modeled and observed cumulative distribution function (CDF) for storm translation speed. Values are the storm translation speed at the time it was nearest to the center of a 250-km radius circle centered on the point indicated by the title of each graph. Observations are shown by black dots, modeled values are shown by red line, and 95% confidence bounds are shown by dashed black lines. Western Gulf of Mexico coastline is shown by blue line for orientation purposes.

https://doi.org/10.5194/wes-2024-123
Preprint. Discussion started: 28 October 2024

eawe european academy of wind energy
Open Access WIND ENERGY SCIENCE DISCUSSIONS

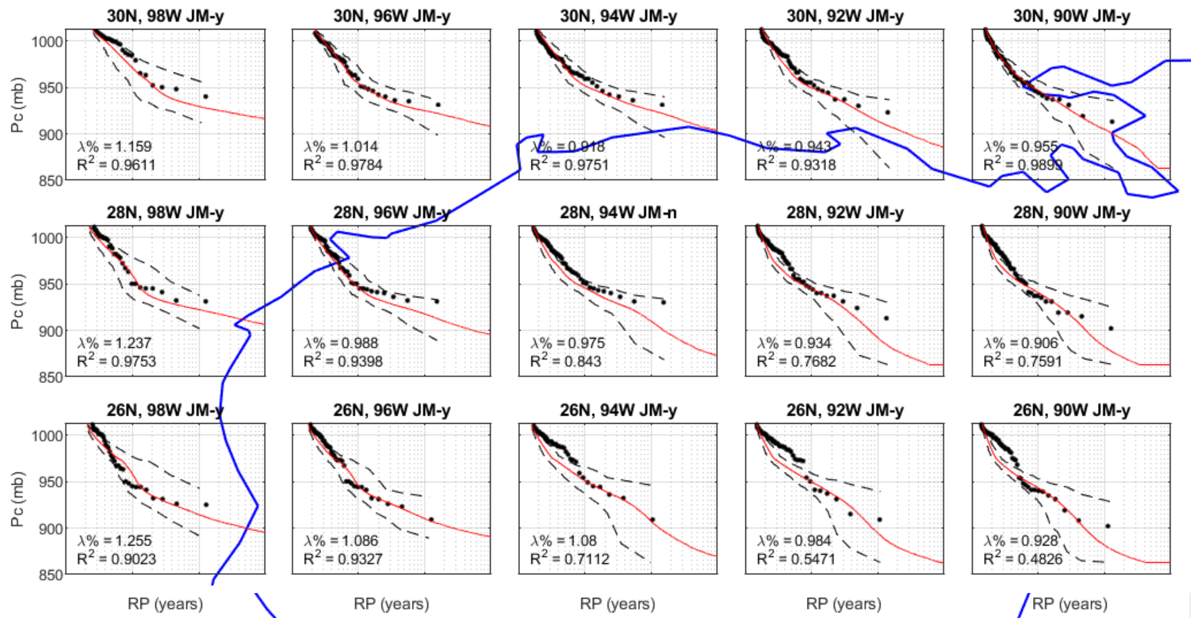

Figure 10. Comparison of modeled and observed central pressure plotted vs. return period. Values correspond to the minimum central pressure given in millibars (mb) while the storm is within a 250-km radius circle centered on the point indicated by the title of each graph. Observations are shown by black dots, modeled values are shown by red line, and 95% confidence bounds are shown by dashed black lines. Western Gulf of Mexico coastline is shown by blue line for orientation purposes. Note J-M-y indicates the modeled central pressures pass the 95% confidence test using the James-Mason test.

In addition to the mean model estimates of pressure vs. return period in each of the plots given in Figure 10, these figures also present the 2.5th and 97.5th percentile (95% confidence range) values of central pressures derived by sampling Np different values of central pressure from the simulated storm set and computing the CDF and then the pressure return period (RP) curve using the model value of λ. This process was repeated 900 times, yielding 900 different RP curves based on sampling Np pressures randomly from the simulated storm set. The 900 different RP curves are then used to define the 95% confidence range for the mean pressure RP curves. In our testing, we include only tropical cyclones with central pressures less than 980 mbar, which is the threshold for a Category 1 event on the Saffir-Simpson hurricane scale. The pc-RP curves yield comparisons that include the combined effects of the modeling of central pressures and the frequency of occurrence of the storms.

Figure 11 presents a comparison of estimates of the landfall pressure as a function of return period. The historical data were obtained from HURDAT2 and Blake et al (2011). The Blake et al. (2011) data include central pressure information from all hurricanes that have made landfall in the United States. HURDAT2 was used to obtain information on the central pressures for all landfalling tropical storms. As in the case of the comparisons of central pressure plotted vs. return period developed from the data passing within 250 km of a given point, each of the plots given in Figure 11 also presents the 2.5th and 97.5th percentile (95% confidence range) values of central pressures derived by resampling. The historical data fall well within the range defined by the 95% confidence bounds.

https://doi.org/10.5194/wes-2024-123
Preprint. Discussion started: 28 October 2024

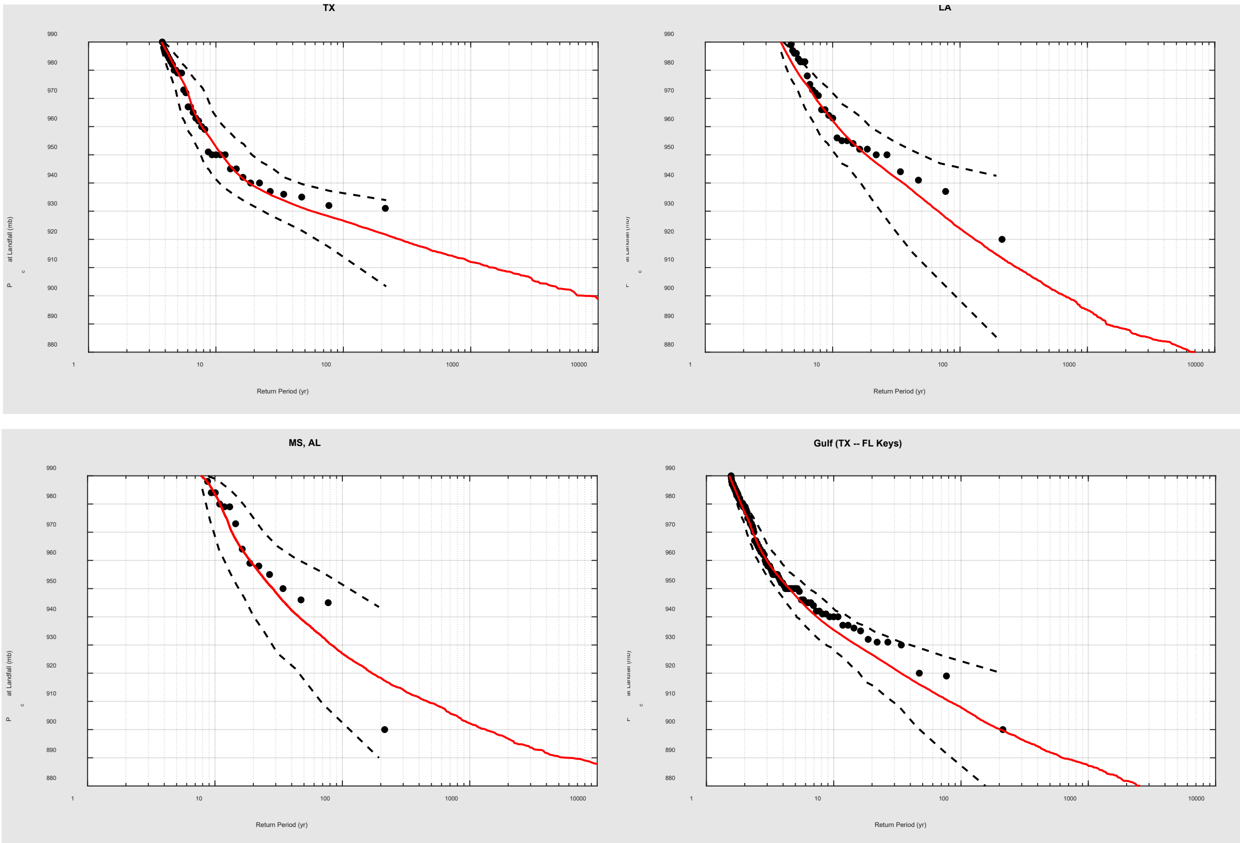

Figure 11. Comparison of modeled and observed central pressures at landfall along the Texas, Louisiana, Mississippi, and Alabama coastlines and the Gulf of Mexico coastline (Texas to Florida Keys). Observations are shown by black dots, modeled values are shown by red line, and 95% confidence bounds are shown by dashed black lines.

3.2 Analysis Methodology

Upon completion of a 500,000-year simulation, the wind speed data are rank ordered and then used to define the wind speed probability distribution, *P(v>V)*, conditional on a storm having passed within 250 km of the site. The probability that the tropical cyclone wind speed (independent of direction) is exceeded during time period *t* is

$$P_t(v > V) = 1 - \sum_{x=0}^{\infty} P(v < V|x)p_t(x) \quad (11)$$

where $P(v < V|x)$ is the probability that velocity v is less than V given that x storms occur, and $p_t(x)$ is the probability of x storms occurring during time period t. $P(v < V|x)$ is obtained by interpolating from the rank-ordered wind speed data. From Equation 12 with $p_t(x)$ defined as Poisson and defining t as 1 year, the annual probability of exceeding a given wind speed is

$$P_a(v > V) = 1 - exp[-\lambda P(v > V)] \quad (12)$$

where λ represents the average annual number of storms approaching within 250 km of the site (i.e., the annual occurrence rate).

https://doi.org/10.5194/wes-2024-123
Preprint. Discussion started: 28 October 2024

3.3 Geospatial Risk Assessment

IEC 61400-1 (IEC TC88-MT1 2019) defines the reference wind speed as a 10-minute average wind speed with a return period of 50 years at turbine hub height. The reference wind speed values for Class 1A and Typhoon Class are provided in Table 1 of IEC 61400-1 as 111.9 and 127.5 mph (50 and 57 m/s), respectively.

Here, we estimated return periods associated with the IEC Class 1A and Typhoon Class limit-state hurricanes on a nominal 10-km by 10-km grid covering the Gulf of Mexico offshore resource area as shown in Figure 12 and Figure 13, respectively. Hub height was assumed to be 150 m, which is typical for the 15-MW class turbines that may be deployed and is the hub height of the National Renewable Energy Laboratory (NREL) 15-MW reference turbine (Gaertner et al. 2020). The wind speed at hub height is needed for comparison with the IEC 61400 design standards. The return period associated with the Class 1A limit state ranges from approximately 20 to 45 years whereas the return period associated with the Typhoon Class limit state ranges from approximately 40 to 110 years.

The 10-minute average wind speed with a return period of 50 years at turbine hub height obtained from the 500,000-year simulation is also presented on the same grid in Figure 14. The figure indicates that the reference wind speed across the Gulf of Mexico offshore resource area ranges from approximately 114 to 132 mph (51 to 59 m/s). Isoclines are also plotted corresponding to the IEC Class 1A and Typhoon Class design limit states. Note that no isocline for the Class 1A limit state appears on the plot of 50-year wind speeds because all 50-year wind speed values obtained from the simulation are greater than the Class 1A reference wind speed (111.9 mph, 50 m/s).

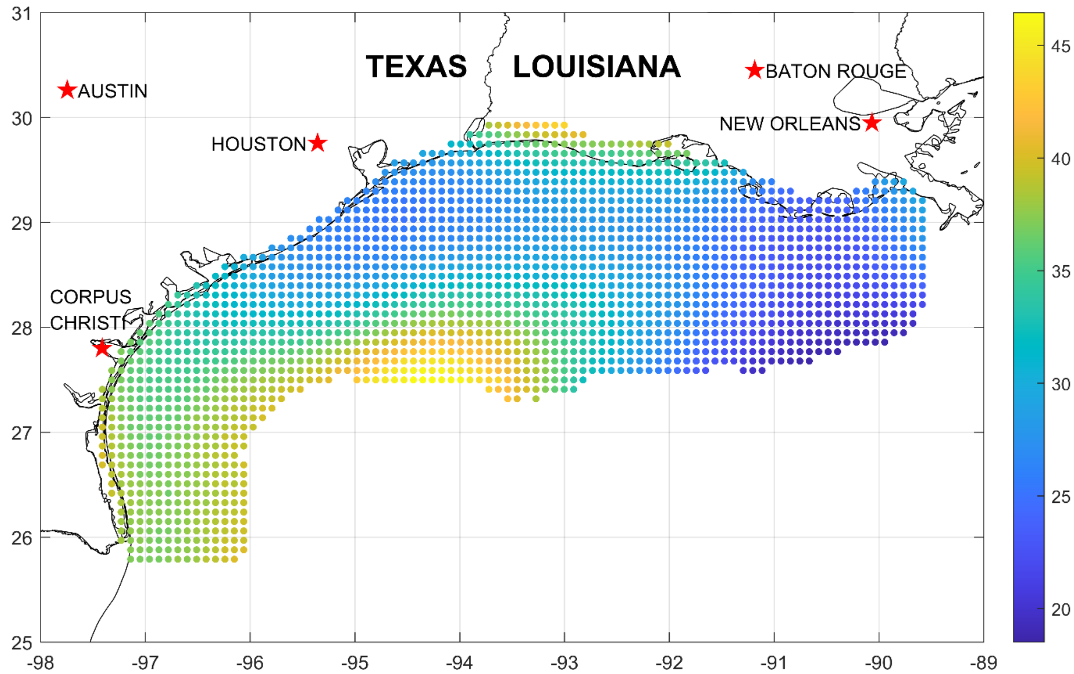

Figure 12: Return period (years) associated with the IEC Class 1A limit-state reference wind speed of 111.9 mph (50 m/s) obtained from a 500,000-year hurricane simulation..

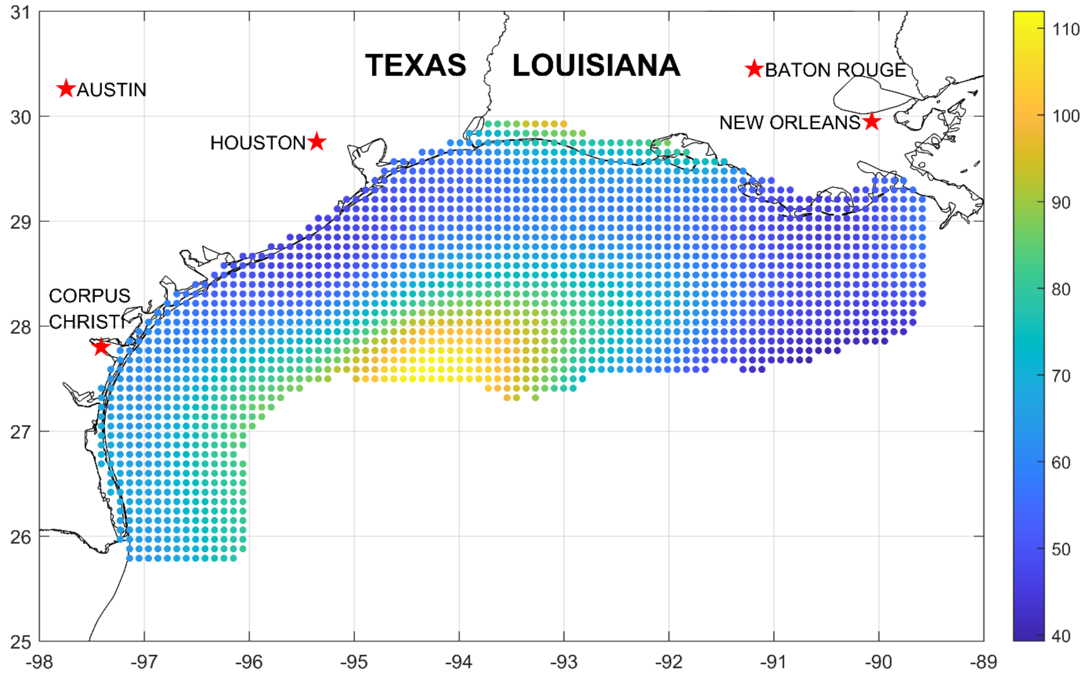

Figure 13: Return period (years) associated with the IEC Typhoon Class limit-state reference wind speed of 127.5 mph (57 m/s) obtained from a 500,000-year hurricane simulation.

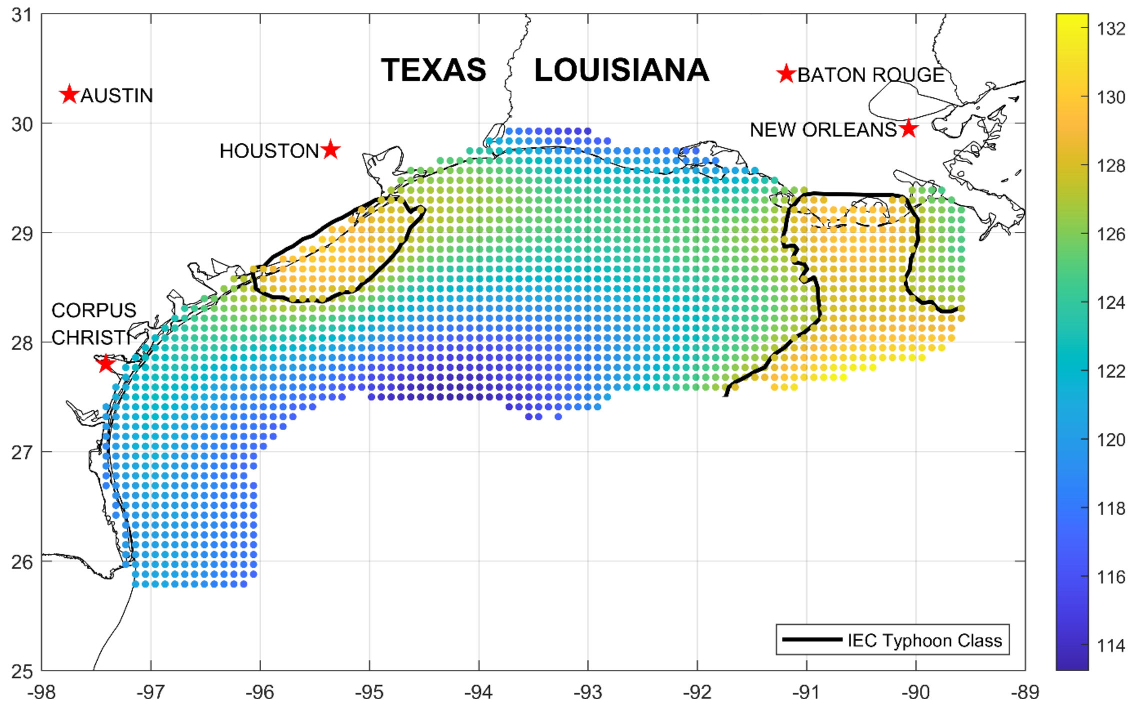

460 **Figure 14: Ten-minute sustained wind speed (mph) at 150 m with a return period of 50 years obtained from a 500,000-year hurricane simulation. Note: No isocline for the Class 1A limit state appears because all simulated values of the 50-year wind speed are greater than the Class 1A reference wind speed (111.9 mph, 50 m/s).**

https://doi.org/10.5194/wes-2024-123
Preprint. Discussion started: 28 October 2024

4 Summary

A challenge in relating a given hurricane event to the IEC design criteria stems from inconsistent hurricane wind speed terminology between the Saffir-Simpson hurricane scale, used by the National Hurricane Center to estimate the intensity of hurricanes, and IEC design criteria used for the design of turbines. Using the latest research on turbulence characteristics of the hurricane boundary layer, definitions of the Saffir-Simpson wind speed scale are provided in Section 2.3 for four averaging times (e.g., 3 seconds, 1 minute, 10 minutes, and 1 hour) and two heights (e.g., 10 m and 150 m). In the same section, definitions of the Class 1A and Typhoon Class limit states are provided in terms of an equivalent Saffir-Simpson category.

For the boundary layer model used, we compared the relationship between the maximum 1-minute wind speeds at the Saffir-Simpson hurricane category break points at 10-m height and wind speeds associated with 3-ssecond averaging times used by IEC wind turbine design standards at 150-m height. The 70-m/s 3-second gust for Class 1A turbines was found to be associated with a strong Category 2 hurricane, and the 80-m/s 3-second gust for Typhoon Class turbines was found to be associated with a moderate Category 3 hurricane.

Using the hurricane hazard model outlined herein, the wind hazard for the Gulf of Mexico Offshore Wind Energy area was defined on a grid with nominal resolution of 10 km. Results of the geospatial risk assessment are provided in Section 3.3. The IEC prescribes the reference wind speeds associated with Class 1A and Typhoon Class limit states to be 50 years, though the return periods associated with the Class 1A limit state were found to range from approximately 20 to 45 years, while the return period associated with the Typhoon Class limit state ranges from approximately 40 to 110 years. This indicates that the Class 1A limit state may be nonconservative for the entire Gulf of Mexico Offshore Wind Energy area, while the Typhoon Class limit state may be adequate for the design of turbines in some regions of the Gulf of Mexico Offshore Wind Energy area. A map of the 10-minute mean wind speeds at 150-m height associated with a return period of 50 years is also provided. The 50-year value was found to range from approximately 114 to 132 mph (51 to 59 m/s).

Competing Interests

The contact author has declared that none of the authors has any competing interests.

References

Andreas, E. L. 2004. "Spray Stress Revisited." *Journal of Physical Oceanography* 34, 1429–1440, https://doi.org/10.1175/1520-0485(2004)034<1429:SSR>2.0.CO;2

Blake, E. S., C. W. Landsea, and E. J. Gibney. 2011. "The deadliest, costliest, and most intense United States tropical cyclones from 1851 to 2010 (and other frequently requested hurricane facts)." NOAA Technical Memorandum NWS NHC-

https://doi.org/10.5194/wes-2024-123
Preprint. Discussion started: 28 October 2024

6, National Weather Service, National Hurricane Center, Miami, Florida, August, 47 pp. www.nhc.noaa.gov/pdf/nws-nhc-6.pdf.

Curcic, M. and B. K. Haus. 2020. Revised estimates of ocean surface drag in strong winds. Geophysical Research Letters, 47, e2020GL087647. https://doi.org/10.1029/2020GL087647.

DeMaria, M. and J. Kaplan 1999. "An updated Statistical Hurricane Intensity Prediction Scheme (SHIPS) for the Atlantic and Eastern North Pacific Basins." *Weather and Forecasting* 14: 326–337, https://doi.org/10.1175/1520-0434(1999)014<0326:AUSHIP>2.0.CO;2

Donelan, M. A. 2018. "On the decrease of the oceanic drag coefficient in high winds." *Journal of Geophysical Research: Oceans* 123: 1485–1501. https://doi.org/10.1002/2017JC013394.

Donelan, M. A., B. K. Haus, N. Reul, W. J. Plant, M. Stiassnie, H. C. Graber, O. B. Brown, and E. S. Saltzman. 2004. "On the limiting aerodynamic roughness of the ocean in very strong winds." *Geophys. Res. Lett.* 31, L18306. doi:10.1029/2004GL019460.

Emanuel, K. A. 1988. "The Maximum Intensity of Hurricanes." *Journal of the Atmospheric Sciences* 45: 1143–1155,https://doi.org/10.1175/1520-0469(1988)045<1143:TMIOH>2.0.CO;2

Emanuel, K. A, S. Ravela, E. Vivant, and C. Risi. 2006. "A statistical–deterministic approach to hurricane risk assessment." *Bull. Amer. Meteor. Soc.* 19: 299–314, https://doi.org/10.1175/BAMS-87-3-299

ESDU. 1982. "Strong Winds in the Atmospheric Boundary Layer, Part 1: Mean Hourly Wind Speed." Engineering Sciences Data Unit Item Number 82026, London, England.

ESDU. 1983. "Strong Winds in the Atmospheric Boundary Layer, Part 2: Discrete Gust Speeds." Engineering Sciences Data Unit Item Number 83045, London, England.

Gao, Z., S. Zhou, J. Zhang, Z. Zeng, and X. Bi. 2021. "Parameterization of sea surface drag coefficient for all wind regimes using 11 aircraft eddy-covariance measurement databases." *Atmosphere*, 12: 1485. https://doi.org/10.3390/atmos12111485.

Gaertner, Evan, Jennifer Rinker, Latha Sethuraman, Frederik Zahle, Benjamin Anderson, Garrett Barter, Nikhar Abbas, Fanzhong Meng, Pietro Bortolotti, Witold Skrzypinski, George Scott, Roland Feil, Henrik Bredmose, Katherine Dykes, Matt Shields, Christopher Allen, and Anthony Viselli. 2020. *Definition of the IEA Wind 15-Megawatt Offshore Reference Wind*. Golden, CO: National Renewable Energy Laboratory (NREL). NREL/TP-5000-75698. https://www.nrel.gov/docs/fy20osti/75698.pdf.

He, J. Y., Q. S. Li, and P. W. Chan. 2020. "Reduced gust factor for extreme tropical cyclone winds over ocean." *J. Wind Eng. Ind. Aerod.* 208: 2–9, https://doi.org/10.1016/j.jweia.2020.104445

Hock, T. R. and J. L. Franklin. 1999. "The NCAR GPS dropwindsonde." *Bull. Am. Meteorol. Soc.* 80: 407–420. https://doi.org/10.1175/1520-0477(1999)080<0407:TNGD>2.0.CO;2

Holland, G. J. 1980. "An analytic model of the wind and pressure profiles in hurricanes." *Mon. Wea. Rev.* 108: 1212–1218, , https://doi.org/10.1175/1520-0493(1980)108<1212:AAMOTW>2.0.CO;2

https://doi.org/10.5194/wes-2024-123
Preprint. Discussion started: 28 October 2024

Holland, G. J., J. I. Belanger, and A. Fritz. 2010. "A revised model for radial profiles of hurricane winds." *Mon. Weather Rev.* 138, 4393–4401, https://doi.org/10.1175/2010MWR3317.1

Holthuijsen, L. H., M. D. Powell, and J. D. Pietrzak. 2012. "Wind and waves in extreme hurricanes." *J. Geophys. Res.* 117: C09003. doi:10.1029/2012JC007983.

Hsu, J.-Y., R. Lien, E. A. D'Asaro, and T. B. Sanford. 2019. "Scaling of drag coefficients under five tropical cyclones." *Geophys. Res. Lett.* 46: 3349–3358. https://doi.org/10.1029/2018GL081574.

IEC TC88-MT1. 2019. *IEC 61400-1 Ed.4. Wind Energy Generation Systems. Part 1: Design Requirements.* International Electrotechnical Commission: Geneva, Switzerland.

Jarosz, E., D. A. Mitchell, D. W. Wang, and W. J. Teague. 2007. "Bottom-up determination of air-sea momentum exchange under a major tropical cyclone." *Science* 315: 1707–1709. doi: 10.1126/science.1136466.

Kepert, J. 2001. "The dynamics of boundary layer jets within the tropical cyclone core. Part I: Linear theory. *J. Atmos. Sci.*, 58, 2469-2484, https://doi.org/10.1175/1520-0469(2001)058<2469:TDOBLJ>2.0.CO;2

Landsea, C. W. and J. L. Franklin. 2013. "Atlantic Hurricane Database Uncertainty and Presentation of a New Database Format." *Mon. Weather Rev.* 141: 3576–3592, https://doi.org/10.1175/MWR-D-12-00254.1

Large, W. G. and S. Pond (1981) Open Ocean Momentum Flux Measurements in Moderate to Strong Winds, *J. Phys. Oceanogr.* **11**, 324-336, https://doi.org/10.1175/1520-0485(1981)011<0324:OOMFMI>2.0.CO;2

Lee, W., S.-H. Kim, I.-L. Moon, M. M. Bell, and I. Ginis. 2022. "New parameterization of air-sea exchange coefficients and its impact on intensity prediction under major tropical cyclones." *Front. Mar. Sci.* 9: 1046511. doi: 10.3389/fmars.2022.1046511.

Liu, B., C. Guan, and L. Xie. 2012. "The wave state and sea spray related parameterization of wind stress applicable from low to extreme winds." *J. Geophys. Res.* 117: C00J22. doi:10.1029/2011JC00778.

Makin, V. K. 2005. "A note on the drag of the sea surface at hurricane winds." *Boundary-Layer Meteorology* 115: 169–176, https://doi.org/10.1007/s10546-004-3647-x

Peng, S. and Y. Li. 2015. "A parabolic model of drag coefficient for storm surge simulation in the South China Sea." *Sci. Rep.* 5: 15496. doi: 10.1038/srep15496.

Powell, M. D., P. J. Vickery, and T. A. Reinhold. 2003. "Reduced drag coefficient for high wind speeds in tropical cyclones." *Nature* 422: 279–283. doi:10.1038/nature01481.

Powell M., G. Soukup, S. Cocke, S. Gulati, N. Morisseau-Leroy, S. Hamid, N. Dorst, and L. Axe, 2005, "State of Florida hurricane loss projection model: Atmospheric science component", *J. Wind Eng. Ind. Aerodyn.* 93, 651-674, https://doi.org/10.1016/j.jweia.2005.05.008

Rayner, N. A., D. E. Parker, E. B. Horton, C. K. Folland, L. V. Alexander, D. P. Rowell, E. C. Kent, and A. Kaplan. 2003. "Global analyses of sea surface temperature, sea ice, and night marine air temperature since the late nineteenth century." *Journal of Geophysical Research* 108(D14): 4407. 10.1029/2002JD002670.

https://doi.org/10.5194/wes-2024-123
Preprint. Discussion started: 28 October 2024

Richter, D. H., R. Bohac, and D. P. Stern. 2016. "An assessment of the flux Profile method for determining air–sea momentum and enthalpy fluxes from dropsonde data in tropical cyclones." *J. Atmos. Sci.* 73: 2665–2682. doi:10.1175/JAS-D-15-0331.1.

Richter, D. H., C. Wainwright, D. P. Stern, G. H. Bryan, and D. Chavas. 2021. "Potential low bias in high-wind drag coefficient inferred from dropsonde data in hurricanes." *J. Atmos. Sci.* 78: 2339–2352.

Shi, J., Z. Zhong, X. Li, G. Jiang, W. Zeng, and Y. Li. 2016. "The Influence of wave state and sea spray on drag coefficient from low to high wind speeds." *Journal of Ocean University of China* 15: 41–49. doi: 10.1007/s11802-016-2655-z.

Smith, R. K. and M. T. Montgomery. 2010. "Hurricane boundary-layer theory." *Q. J. R. Meteorol. Soc.* 136: 1665–1670. doi:10.1002/qj.679.

Smith R. K. and M. T. Montgomery. 2014. "On the existence of the logarithmic surface layer in the inner core of hurricanes." *Quart. J. Roy. Meteor. Soc.* 140: 72–81. https://doi.org/10.1002/qj.2121.

Takagaki, N., S. Komori, N. Suzuki, K. Iwano, T. Kuramoto, S. Shimada, R. Kurose, and K. Takahashi. 2012. "Strong correlation between the drag coefficient and the shape of the wind sea spectrum over a broad range of wind speeds." *Geophys. Res. Lett.* 39: L23604. doi:10.1029/2012GL053988.

Thompson, E. F. and V. J. Cardone, 1996. "Practical Modeling of Hurricane Surface Wind Fields", *J. Wtrwy., Port, Coast., and Oc. Engrg.*. 122, 195-205

Troitskaya, Y. I., D. A. Sergeev, A. A. Kandaurov, G. A. Baidakov, M. A. Vdovin, and V. I. Kazakov. 2012. "Laboratory and theoretical modeling of air-sea momentum transfer under severe wind conditions." *J. Geophys. Res.* 117: C00J21. doi:10.1029/2011JC007778.

Vickers, D., L. Mahrt, and E. L. Andreas. 2013. "Estimates of the 10-m neutral sea surface drag coefficient from aircraft eddy-covariance measurements." *J. Phys. Oceanogr.* 43(2): 301–310, https://doi.org/10.1175/JPO-D-12-0101.1

Vickery, P. J., P. F. Skerlj, A. C. Steckley, and L. A. Twisdale, 2000a. "Hurricane Wind Field Model for Use in Hurricane Simulations", *J. Struct. Engrg.,* 10, 1203-1221, https://doi.org/10.1061/(ASCE)0733-9445(2000)126:10(1203)

Vickery, P. J., P. F. Skerlj, and L. A. Twisdale, Jr. 2000b. "Simulation of Hurricane Risk in the U.S. Using an Empirical Track Model." *J. Struct. Engrg. , ASCE* 126(), 1222-1237. https://doi.org/10.1061/(ASCE)0733-9445(2000)126:10(1222)

Vickery, P. J. 2005. "Simple Empirical Models for Estimating the Increase in the Central Pressure of Tropical Cyclones after Landfall along the Coastline of the United States." *J. Appl. Meteor.,* 44, 1807–1826.. https://doi.org/10.1175/JAM2310.1

Vickery, P. J. and P. F. Skerlj. 2005. "Hurricane Gust Factors Revisited." *J. Struct. Engrg.* 131(): 825–832, https://doi.org/10.1061/(ASCE)0733-9445(2005)131:5(825)

Vickery, P. J. and D. Wadhera. 2008. "Statistical Models of Holland Pressure Profile Parameter and Radius to Maximum Winds of Hurricanes from Flight Level Pressure and H*Wind Data." *J. Appl. Meteor.* 47: 2497–2517, https://doi.org/10.1175/2008JAMC1837.1

Vickery, P. J., D. Wadhera, M. D. Powell, and Y. Chen. 2009a. "A hurricane boundary layer and wind field model for use in engineering applications." *J. Appl. Meteor.*. 48: 381–405. https://doi.org/10.1175/2008JAMC1841.1.

https://doi.org/10.5194/wes-2024-123
Preprint. Discussion started: 28 October 2024

Vickery, P. J., D. Wadhera, L. A. Twisdale, and F. M. Lavelle. 2009b. "United States Hurricane Wind Speed Risk and Uncertainty." *J. Struct. Engrg.* 135: 301–320, https://doi.org/10.1061/(ASCE)0733-9445(2009)135:3(301)

Ye, L., Y. Li, and Z. Gao. 2022. "Surface layer drag coefficient at different radius ranges in tropical cyclones." *Atmosphere* 13: 280. https://doi.org/10.3390/atmos13020280.

Zou, Z., D. Zhao, J. Tian, B. Liu, and J. Huang. 2018. "Drag coefficients derived from ocean current and temperature profiles at high wind speeds." *Tellus A: Dynamic Meteorology and Oceanography* 70(1): 1–13, doi: 10.1080/16000870.2018.1463805.